



## Open Archive Toulouse Archive Ouverte

OATAO is an open access repository that collects the work of Toulouse researchers and makes it freely available over the web where possible

This is an publisher's version published in: <http://oatao.univ-toulouse.fr/22981>

### Official URL:

<https://doi.org/10.1016/j.compfluid.2018.09.014>

### To cite this version:

Odier, Nicolas and Sanjosé, Marlène and Gicquel, Laurent and Poinot, Thierry and Moreau, Stéphane and Duchaine, Florent A characteristic inlet boundary condition for compressible, turbulent, multispecies turbomachinery flows. (2019) Computers and Fluids, 178. 41-55. ISSN 0045-7930

Any correspondence concerning this service should be sent to the repository administrator: [tech-oatao@listes-diff.inp-toulouse.fr](mailto:tech-oatao@listes-diff.inp-toulouse.fr)

# A characteristic inlet boundary condition for compressible, turbulent, multispecies turbomachinery flows

Nicolas Odier<sup>a,\*</sup>, Marlène Sanjosé<sup>b</sup>, Laurent Gicquel<sup>a</sup>, Thierry Poinso<sup>a</sup>, Stéphane Moreau<sup>b</sup>, Florent Duchaine<sup>a</sup>

<sup>a</sup>CFD Team, CERFACS, Toulouse 31057, France

<sup>b</sup>University of Sherbrooke, Sherbrooke QC J1K 2R1, Canada

## A B S T R A C T

A methodology to implement non-reflecting boundary conditions for turbomachinery applications, based on characteristic analysis is described in this paper. For these simulations, inlet conditions usually correspond to imposed total pressure, total temperature, flow angles and species composition. While directly imposing these quantities on the inlet boundary condition works correctly for steady RANS simulations, this approach is not adapted for compressible unsteady Large Eddy Simulations because it is fully reflecting in terms of acoustics. Deriving non-reflecting conditions in this situation requires to construct characteristic relations for the incoming wave amplitudes. These relations must impose total pressure, total temperature, flow angle and species composition, and simultaneously identify acoustic waves reaching the inlet to let them propagate without reflection. This treatment must also be compatible with the injection of turbulence at the inlet. The proposed approach shows how characteristic equations can be derived to satisfy all these criteria. It is tested on several cases, ranging from a simple inviscid 2D duct to a rotor/stator stage with turbulence injection.

### Keywords:

Characteristic inlet boundary condition  
Turbomachinery inflow conditions  
Compressible flow  
Turbulence injection  
Acoustic reflectivity

## 1. Introduction

Specifying inlet and outlet boundary conditions for compressible simulation still remains a key issue (Colonius [8]) especially for unsteady flows where wave reflections must be controlled. In this field, characteristic boundary conditions have progressively become standard. Initially introduced by Thompson [48], Euler Characteristic Boundary Conditions (ECBC) was then extended by Poinso and Lele [34] to viscous flows by proposing the Navier–Stokes Characteristic Boundary Conditions (NSCBC) approach. This method specifies a given number of quantities –for example static pressure for an outlet, velocity and temperature for an inlet– on the boundary condition, and allowing the outgoing waves, computed by the numerical scheme, to leave the domain with minimum reflection. The NSCBC strategy has been later extended to multi-species reacting flows and to aeroacoustics (Baum et al. [3], Okong'o and Bellan [31], Moureau et al. [29], Poinso and Veynante [33], Yoo et al. [53], Yoo and Im [52], Freund [13], Colonius [7]).

The NSCBC original paper [34] provides examples of implementations for several boundary conditions. A subsonic inflow spec-

ifying the three velocity components and the static temperature is detailed, and remains today a very common boundary condition for most applications. Later, Guézennec and Poinso [19] proposed a modification of this inlet condition to yield the vortical-flow characteristic boundary condition (VFCBC), based on a Mach number expansion detailed in Prosser [38]. This VFCBC allows vorticity wave injections while acoustics waves propagate outside the domain without reflection.

While characteristics boundaries are required for LES and DNS of reacting flows or aeroacoustic applications, they are much less used for turbomachinery simulations.

- At outlets, most turbomachinery simulations use today an imposed static pressure profile satisfying an approximate radial momentum equation also termed simplified radial equilibrium. This boundary condition is however and by construction fully reflecting, and therefore not adequate for proper LES and DNS of such flows. In 2014, Koupper et al. [21] have shown that the NSCBC methodology remains fully compatible with turbomachinery computations in stator vanes allowing both radial equilibrium to occur while being non-reflective.
- At inlets, turbomachinery conditions usually correspond to imposed total pressure  $P_t = P_s \left(1 + \frac{\gamma-1}{2} M^2\right)^{\frac{\gamma}{\gamma-1}}$ , total temperature

\* Corresponding author.

E-mail address: nicolas.odier@cerfacs.fr (N. Odier).

$T_t = T_s \left(1 + \frac{\gamma-1}{2} M^2\right)$ , where  $P_s$  is the static pressure,  $T_s$  is the static temperature,  $M$  the Mach number,  $\gamma$  the adiabatic coefficient, as well as flow direction, and species mass fractions. The use of total temperature and pressure for turbomachinery applications lies in the fact that the total quantity losses correspond to exchanged work and heat transfer of such systems. These quantities are also commonly measured at different sections in test engine using Pitot tubes and thermocouples. For Euler equations and steady flows, Giles [16] and Saxer and Giles [40] proposed a total quantity inflow formulation, later extended to 3D flows by Anker et al. [2], and to unsteady flows by Schluß et al. [41]. For unsteady Navier–Stokes equations, Struijs et al. [45] also reported a NSCBC formulation to impose total pressure, total temperature, and flow angle. Their chosen formulation however relies on an incompressible definition of the total pressure which is invalid for compressible flows.

- Aside from adequately prescribing the total quantities while treating acoustic, an inlet turbomachinery boundary condition must be able to handle vorticity injection. Indeed turbulence may have a significant impact on turbomachinery flows (Choi et al. [5], Carullo et al. [4]). For a fan or a compressor computation, the level of turbulence is likely to modify the suction side transition mode, which will influence losses predictions (Jahanmiri [20], Wissink et al. [50], Michelassi et al. [27], Scillitoe et al. [43]).

The aim of this paper is thus to propose a NSCBC inlet boundary condition imposing total pressure, total temperature, flow direction, and composition in a compressible context, and which is compatible with turbulence injection for both Direct Numerical Simulation (DNS) and Large Eddy Simulation (LES). The paper is organized as follows: Section 2 describes the NSCBC formulation for this inlet condition. Section 3 evaluates the methodology on several test-cases, from academic test-cases to complex industrial configurations. For all cases, the outlet condition is a fixed static pressure, imposed through a NSCBC methodology.

## 2. NSCBC strategy to impose $P_t$ , $T_t$ , directions and species composition

### 2.1. The NSCBC methodology

This subsection summarizes the main ideas of the NSCBC strategy. For more details, the reader is referred to Thompson [48], Giles [15] (Euler equations), Poinso and Lele [34], Poinso and Veynante [33] (Navier–Stokes equations), Nicoud [30] (Euler and Navier–Stokes equations).

The compressible Navier–Stokes equations, using Einstein notation, are:

$$\frac{\partial \rho}{\partial t} + \frac{\partial}{\partial x_i} (\rho u_i) = 0 \quad (1)$$

$$\frac{\partial \rho u_i}{\partial t} + \frac{\partial}{\partial x_j} (\rho u_i u_j) + \frac{\partial P_s}{\partial x_i} = \frac{\partial \tau_{ij}}{\partial x_j} \quad (2)$$

$$\frac{\partial \rho E}{\partial t} + \frac{\partial}{\partial x_i} (\rho E + P_s) u_i = \frac{\partial}{\partial x_i} (u_j \tau_{ij}) - \frac{\partial q_i}{\partial x_i} \quad (3)$$

where  $\rho$  is the local fluid density,  $u_i$  the velocity components,  $P_s$  the static pressure,  $T_s$  the static temperature,  $E$  the total energy, and  $\tau_{ij}$  the stress tensor defined as:

$$\tau_{ij} = \mu \left( \frac{\partial u_i}{\partial x_j} + \frac{\partial u_j}{\partial x_i} - \frac{2}{3} \delta_{ij} \frac{\partial u_k}{\partial x_k} \right) \quad (4)$$

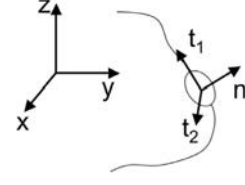


Fig. 1. Rotation from cartesian basis to the normal patch basis.

with  $\delta_{ij}$  the Kronecker delta and  $\mu$  the dynamic viscosity.  $q_i$  is the heat flux along the  $x_i$  direction and is defined as  $q_i = -\lambda \frac{\partial T_s}{\partial x_i}$ , where  $\lambda$  is the thermal conductivity. The system is finally closed using the ideal gas law:

$$P_s = \rho r T_s \quad (5)$$

where  $r$  is the specific gas constant of the mixture  $r = \frac{R}{W}$ , with  $W$  the mean molecular weight of the mixture and  $R = 8.3143 \text{ J/mol.K}$  the universal gas constant.

The present paper focuses on Direct Numerical Simulations (DNS), where all energetic scales are resolved, or on Large Eddy Simulations (LES) (Leonard [24], Germano [14]). In terms of boundary conditions, using DNS or LES leads to the same solution. The first step to build characteristic boundary conditions is to write all equations in a reference frame linked to the boundary surface, where the normal vector is noted  $\vec{n}$ , and the two tangential vectors are respectively noted as  $\vec{t}_1$  and  $\vec{t}_2$  (Fig. 1).

The characteristic analysis of Thompson [48] for Euler equations consists in transforming the conservative variables  $\mathbf{U} = (\rho \mathbf{u}, \rho \mathbf{v}, \rho \mathbf{w}, \rho \mathbf{E})^T$  into primitive variables in the reference frame  $(\vec{n}, \vec{t}_1, \vec{t}_2)$  so that we get:  $\mathbf{V} = (\mathbf{u}_n, \mathbf{u}_{t_1}, \mathbf{u}_{t_2}, P_s, \rho \mathbf{k})^T$ . Then transforming those primitives variables into characteristics variables, it results from both operations conservative variables  $\mathbf{U}$  which satisfy:

$$\frac{\partial \mathbf{U}}{\partial t} + \mathbf{A}_U \frac{\partial \mathbf{U}}{\partial x} + \mathbf{B}_U \frac{\partial \mathbf{U}}{\partial y} + \mathbf{C}_U \frac{\partial \mathbf{U}}{\partial z} + \mathbf{S} = \mathbf{0} \quad (6)$$

where  $\mathbf{A}_U, \mathbf{B}_U, \mathbf{C}_U$  are the Jacobian matrices of the respective fluxes in the  $x, y,$  and  $z$  directions, and  $\mathbf{S}$  is the diffusion term. Similarly, the primitives variables  $\mathbf{V}$  satisfy:

$$\frac{\partial \mathbf{V}}{\partial t} + \mathbf{N} \frac{\partial \mathbf{V}}{\partial n} + \mathbf{T}_1 \frac{\partial \mathbf{V}}{\partial t_1} + \mathbf{T}_2 \frac{\partial \mathbf{V}}{\partial t_2} + \mathbf{S} = \mathbf{0} \quad (7)$$

where  $\mathbf{N}$  is the normal Jacobian,  $\mathbf{T}_1$  and  $\mathbf{T}_2$  are the two tangential Jacobian along  $\vec{t}_1$  and  $\vec{t}_2$ . The transformation of the primitives variables into normal characteristics variables consists in diagonalizing the Jacobian  $\mathbf{N}$  and writing the balance equations for the characteristic variables  $\mathbf{W}$ :

$$\frac{\partial \mathbf{W}}{\partial t} + \mathbf{D} \frac{\partial \mathbf{W}}{\partial n} = \mathbf{S}_W - \mathbf{T}_W \quad (8)$$

$\mathbf{D}$  is thus a diagonal matrix containing the characteristic propagation velocities  $\lambda_i$  (eigenvalues of  $\mathbf{N}$ ), and  $\mathbf{S}_W - \mathbf{T}_W$  is the sum of all the non-hyperbolic, non-normal to the boundary condition terms: reaction, diffusion, and tangential terms.

The notation  $\mathcal{L}_i = \lambda_i \frac{\partial \mathbf{W}}{\partial n}$  is introduced to characterize the wave amplitude associated with each characteristic velocities  $\lambda_i$ , where  $i$  is the index of the corresponding wave. The characteristic analysis applied to the Navier–Stokes equations finally leads to the characteristic  $\mathcal{L}_i$  waves (Fig. 2), written in the boundary reference frame  $(\vec{n}, \vec{t}_1, \vec{t}_2)$  (Poinso and Lele [34]):

$$\begin{pmatrix} \mathcal{L}_+ \\ \mathcal{L}_- \\ \mathcal{L}_{t_1} \\ \mathcal{L}_{t_2} \\ \mathcal{L}_S \end{pmatrix} = \begin{pmatrix} (u_n + c) \left( \frac{\partial u_n}{\partial n} + \frac{1}{\rho c} \frac{\partial P_s}{\partial n} \right) \\ (u_n - c) \left( -\frac{\partial u_n}{\partial n} + \frac{1}{\rho c} \frac{\partial P_s}{\partial n} \right) \\ u_n \frac{\partial u_{t_1}}{\partial n} \\ u_n \frac{\partial u_{t_2}}{\partial n} \\ u_n \left( \frac{\partial \rho}{\partial n} - \frac{1}{c^2} \frac{\partial P_s}{\partial n} \right) \end{pmatrix} \quad (9)$$

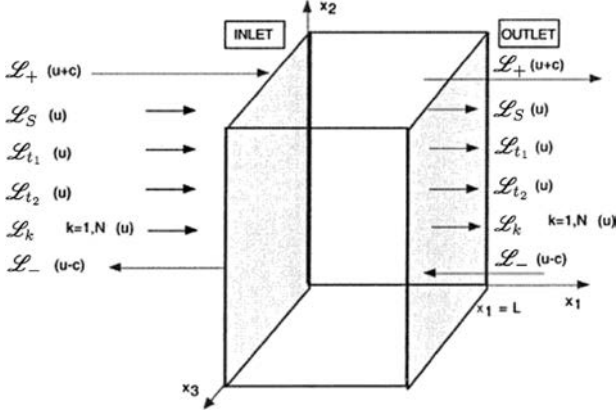


Fig. 2. Inlet and outlet boundary conditions, and respective  $\mathcal{L}_i$  waves.

$\mathcal{L}_+$  and  $\mathcal{L}_-$  are respectively the inward and the outward acoustic waves, while  $\mathcal{L}_{t_1}$  and  $\mathcal{L}_{t_2}$  are transverse shear waves, and  $\mathcal{L}_S$  is the entropic wave. Species waves  $\mathcal{L}_k$  may also be introduced as:

$$\mathcal{L}_S = \sum_{k=1}^N \mathcal{L}_k \quad \text{with} \quad \mathcal{L}_k = \frac{\partial \rho_k}{\partial n} - \frac{Y_k}{c^2} \frac{\partial P_s}{\partial n} \quad (10)$$

where  $\rho_k$  is the density of species  $k$ , and  $Y_k$  the mass fraction of species  $k$ .

The NSCBC strategy consists in considering a locally one-dimensional inviscid (LODI) flow on the boundary to specify the amplitude of ingoing waves. The characteristic system for the Navier–Stokes equations hence becomes after the LODI assumptions:

$$\frac{\partial \rho}{\partial t} + \left( \mathcal{L}_S + \frac{\rho c}{2} (\mathcal{L}_+ + \mathcal{L}_-) \right) = 0 \quad (11)$$

$$\frac{\partial P_s}{\partial t} + \frac{\rho c}{2} (\mathcal{L}_+ + \mathcal{L}_-) = 0 \quad (12)$$

$$\frac{\partial u_n}{\partial t} + \frac{1}{2} (\mathcal{L}_+ - \mathcal{L}_-) = 0 \quad (13)$$

$$\frac{\partial u_{t_1}}{\partial t} + \mathcal{L}_{t_1} = 0 \quad (14)$$

$$\frac{\partial u_{t_2}}{\partial t} + \mathcal{L}_{t_2} = 0 \quad (15)$$

Note that these LODI relations may be combined to express the time derivatives of other quantities (Appendix 5.1). Waves amplitudes are deduced using LODI relations (Poinsot and Lele [34]), and then used on the boundary in Eq. (7) to advance the solution in time. In terms of treatment, specifying the ingoing wave amplitudes is actually the crucial part of most NSCBC extensions and LODI formulations have been improved to account for transverse terms by Yoo et al. [53], Yoo and Im [52], Lodato et al. [26], and Granet et al. [18].

## 2.2. LODI relations for $P_t$ , $T_t$ , flow direction, and species composition

When the objective of the boundary condition treatment is to impose  $P_t$ ,  $T_t$ , flow direction and species composition at the inlet, the use of NSCBC requires LODI expressions for  $P_t$  and  $T_t$ . This was not done in Poinsot and Lele [34] and it requires some algebra as shown below. To account for compressibility effects, total pressure  $P_t$  and total temperature  $T_t$  need to be expressed as functions of

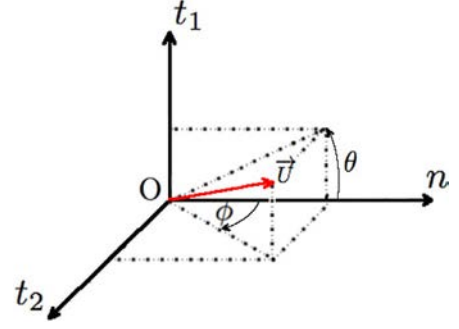


Fig. 3. Velocity vector  $\vec{U}$ , and corresponding  $\theta$  and  $\phi$  angles defining the flow direction.

the local flow Mach number  $M$ . This implies that temporal derivation of  $P_t$  and  $T_t$  will involve the Mach number temporal derivative. This Mach number derivation itself involves the derivation of the kinetic energy equation (Appendix 5.2), due to the relation:

$$M^2 = \frac{u_n^2 + u_{t_1}^2 + u_{t_2}^2}{\gamma r T_s} = \frac{2e_c}{\gamma r T_s} \quad (16)$$

where  $e_c$  is the kinetic energy,  $\gamma$  the adiabatic coefficient,  $r$  is the specific gas constant, and  $T_s$  the static temperature. The adiabatic coefficient  $\gamma$  is considered to be constant. Writing  $\beta = (\gamma - 1)$ , after algebraic manipulations (Appendix 5.3), its temporal derivative is expressed as:

$$\frac{\partial M^2}{\partial t} = \frac{2}{c^2} \left( \mathcal{L}_+ \cdot \left( \frac{\beta e_c}{2c} - \frac{u_n}{2} \right) + \mathcal{L}_- \cdot \left( \frac{\beta e_c}{2c} + \frac{u_n}{2} \right) - u_{t_1} \mathcal{L}_{t_1} - u_{t_2} \mathcal{L}_{t_2} - \frac{e_c}{\rho} \cdot \mathcal{L}_S \right) \quad (17)$$

Using Eq. (17), the total pressure LODI equation becomes (Appendix 5.4):

$$\begin{aligned} \frac{\partial P_t}{\partial t} = & \mathcal{L}_+ \cdot \left( -\frac{\rho c}{2} \frac{P_t}{P_s} + \frac{P_t}{r T_t} \cdot \left( \frac{\beta e_c}{2c} - \frac{u_n}{2} \right) \right) + \mathcal{L}_- \cdot \left( -\frac{\rho c}{2} \frac{P_t}{P_s} \right. \\ & \left. + \frac{P_t}{r T_t} \cdot \left( \frac{\beta e_c}{2c} + \frac{u_n}{2} \right) \right) - \mathcal{L}_{t_1} u_{t_1} \cdot \frac{P_t}{r T_t} - \mathcal{L}_{t_2} u_{t_2} \cdot \frac{P_t}{r T_t} \\ & - \frac{e_c}{\rho} \cdot \mathcal{L}_S \cdot \frac{P_t}{r T_t} \end{aligned} \quad (18)$$

Similarly, the equation for total temperature reads (Appendix 5.5):

$$\begin{aligned} \frac{\partial T_t}{\partial t} = & \mathcal{L}_+ \cdot \left( -\frac{\beta T_t}{2c} + \frac{1}{C_p} \left( \frac{\beta e_c}{2c} - \frac{u_n}{2} \right) \right) + \mathcal{L}_- \cdot \left( -\frac{\beta T_t}{2c} \right. \\ & \left. + \frac{1}{C_p} \left( \frac{\beta e_c}{2c} + \frac{u_n}{2} \right) \right) - \mathcal{L}_{t_1} \frac{u_{t_1}}{C_p} - \mathcal{L}_{t_2} \frac{u_{t_2}}{C_p} \\ & + \frac{T_t}{\rho r} \sum_{k=1}^N r_k \mathcal{L}_k - \frac{e_c}{\rho C_p} \cdot \mathcal{L}_S \end{aligned} \quad (19)$$

where  $C_p = \frac{\gamma r}{\gamma - 1}$  applies. The flow direction is fixed by imposing  $\sin(\theta)$  and  $\sin(\phi)$ , where  $\theta$  and  $\phi$  are respectively the flow angles in the  $(O, \vec{n}, t_1)$  plane and in the  $(O, \vec{n}, t_2)$  plane (Fig. 3). These two specific variables can be linked to the local flow velocity vector since

$$\sin(\theta) = \frac{u_{t_1}}{\|\vec{U}\|}, \quad \sin(\phi) = \frac{u_{t_2}}{\|\vec{U}\|} \quad (20)$$

using:

$$\|\vec{U}\| = \sqrt{u_n^2 + u_{t_1}^2 + u_{t_2}^2} \quad (21)$$

**Table 1**

Summary of characteristic equations to consider to impose total pressure  $P_t$ , total temperature  $T_t$ , flow direction through imposition of  $\theta$  and  $\phi$ , and species composition  $Y_k$ .

Total pressure	$\frac{\partial P_t}{\partial t} = \mathcal{L}_+ \cdot \left( -\frac{\rho c}{2} \frac{P_t}{P_s} + \frac{P_t}{r T_t} \cdot \left( \frac{\beta e_c}{2c} - \frac{u_n}{2} \right) \right)$
LODI equation	$+ \mathcal{L}_- \cdot \left( -\frac{\rho c}{2} \frac{P_t}{P_s} + \frac{P_t}{r T_t} \cdot \left( \frac{\beta e_c}{2c} + \frac{u_n}{2} \right) \right)$ $- \mathcal{L}_{t_1} u_{t_1} \cdot \frac{P_t}{r T_t} - \mathcal{L}_{t_2} u_{t_2} \cdot \frac{P_t}{r T_t}$ $- \frac{e_c}{\rho} \cdot \mathcal{L}_S \cdot \frac{P_t}{r T_t}$
Total temperature	$\frac{\partial T_t}{\partial t} = \mathcal{L}_+ \cdot \left( -\frac{\beta T_t}{2c} + \frac{1}{C_p} \left( \frac{\beta e_c}{2c} - \frac{u_n}{2} \right) \right)$
LODI equation	$+ \mathcal{L}_- \cdot \left( -\frac{\beta T_t}{2c} + \frac{1}{C_p} \left( \frac{\beta e_c}{2c} + \frac{u_n}{2} \right) \right)$ $- \mathcal{L}_{t_1} \frac{u_{t_1}}{C_p} - \mathcal{L}_{t_2} \frac{u_{t_2}}{C_p} + \frac{T_t}{\rho r} \sum_{k=1}^N r_k \mathcal{L}_k$ $- \frac{e_c}{\rho C_p} \cdot \mathcal{L}_S$
Flow direction	$\frac{\partial u_{t_1}}{\partial t} = -\mathcal{L}_{t_1}$
LODI equation	$\frac{\partial u_{t_2}}{\partial t} = -\mathcal{L}_{t_2}$
Species composition LODI equation	$\frac{\partial Y_k}{\partial t} = -\frac{1}{\rho} (\mathcal{L}_k - Y_k \mathcal{L}_S)$

The latter is equivalent to impose the two shear waves, since:

$$\frac{\partial u_{t_1}}{\partial t} = \frac{\partial}{\partial t} \left( \|\vec{U}\| \times (\sin(\theta)) \right) = -\mathcal{L}_{t_1} \quad (22)$$

$$\frac{\partial u_{t_2}}{\partial t} = \frac{\partial}{\partial t} \left( \|\vec{U}\| \times (\sin(\phi)) \right) = -\mathcal{L}_{t_2} \quad (23)$$

Note that with the formalism at hand, the velocity magnitude  $\|\vec{U}\|$  is not imposed, only  $\theta$  and  $\phi$  are imposed through the use of transverse shear waves. Note that Albin et al. [1] proposed to re-write the characteristic equations in a different frame of reference. This approach should not differ from our method since the momentum equations are the same in all frames.

The target  $P_t$  and  $T_t$  may change with time, so that terms  $\frac{\partial P_t}{\partial t}$  and  $\frac{\partial T_t}{\partial t}$  are kept in the LODI equations of Table 1. Finally, the species composition is imposed as :

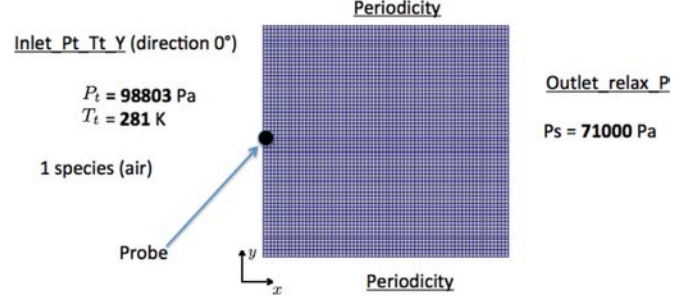
$$\frac{\partial Y_k}{\partial t} = -\frac{1}{\rho} (\mathcal{L}_k - Y_k \mathcal{L}_S) \quad (24)$$

### 2.3. The $P_t - T_t$ NSCBC treatment

Having identified the evolution equations to be considered in the context of the LODI assumptions, the remaining step consists in imposing the desired informations while satisfying specific properties for the boundary condition. As already stated, out of the 5  $\mathcal{L}_i$  in the system, the two shear waves are fixed when imposing the flow angle (Eqs. (22) and (23)). The remaining waves  $\mathcal{L}_+$ ,  $\mathcal{L}_S$  and  $\mathcal{L}_k$  can then be determined solving the system given by Eqs. (18), (19), (24):

$$\begin{aligned} & \mathcal{L}_+ \cdot \left( -\frac{\rho c}{2} \frac{P_t}{P_s} + \frac{P_t}{r T_t} \left( \frac{\beta e_c}{2c} - \frac{u_n}{2} \right) \right) - \mathcal{L}_S \cdot \frac{e_c}{\rho} \frac{P_t}{r T_t} \\ &= \frac{\partial P_t}{\partial t} + \frac{P_t}{r T_t} \cdot (\mathcal{L}_{t_1} u_{t_1} + \mathcal{L}_{t_2} u_{t_2}) \\ & - \mathcal{L}_- \cdot \left( -\frac{\rho c}{2} \frac{P_t}{P_s} + \frac{P_t}{r T_t} \left( \frac{\beta e_c}{2c} + \frac{u_n}{2} \right) \right) \end{aligned} \quad (25)$$

$$\begin{aligned} & \mathcal{L}_+ \cdot \left( -\frac{\beta T_t}{2c} + \frac{1}{C_p} \left( \frac{\beta e_c}{2c} - \frac{u_n}{2} \right) \right) - \frac{e_c}{\rho C_p} \cdot \mathcal{L}_S \\ &= \frac{\partial T_t}{\partial t} + \frac{1}{C_p} \cdot (\mathcal{L}_{t_1} u_{t_1} + \mathcal{L}_{t_2} u_{t_2}) - \frac{T_t}{\rho r} \sum_{k=1}^N r_k \mathcal{L}_k \end{aligned}$$

**Fig. 4.** 2D test case.

$$- \mathcal{L}_- \cdot \left( -\frac{\beta T_t}{2c} + \frac{1}{C_p} \left( \frac{\beta e_c}{2c} + \frac{u_n}{2} \right) \right) \quad (26)$$

$$\frac{\partial Y_k}{\partial t} = -\frac{1}{\rho} (\mathcal{L}_k - Y_k \mathcal{L}_S) \quad (27)$$

### 2.4. Final waves expression

The resolution of the system of Eqs. (25)–(27) is detailed in Appendix 5.6. It yields the following expressions, termed **Pt-Tt-NSCBC-R**:

$$\mathcal{L}_{t_1} = -\frac{\partial u_{t_1}}{\partial t} \quad (28)$$

$$\mathcal{L}_{t_2} = -\frac{\partial u_{t_2}}{\partial t} \quad (29)$$

$$\mathcal{L}_k = Y_k \mathcal{L}_S - \rho \frac{\partial Y_k}{\partial t} \quad (30)$$

$$\begin{aligned} & \mathcal{L}_+ \\ &= \frac{F_1 \frac{\partial T_t}{\partial t} + F_2 \frac{\partial P_t}{\partial t} + \frac{P_t}{r T_t} \cdot F_2 F_3 + \frac{1}{C_p} \cdot F_1 F_3 + F_1 \cdot \frac{T_t}{r} \sum_{k=1}^N r_k \frac{\partial Y_k}{\partial t} - \mathcal{L}_- \cdot (F_2 F_6 + F_1 F_7)}{F_4 F_2 + F_5 F_1} \end{aligned} \quad (31)$$

$$\mathcal{L}_S = \frac{\frac{\partial T_t}{\partial t} + \frac{1}{C_p} F_3 + \frac{T_t}{r} \sum_{k=1}^N r_k \frac{\partial Y_k}{\partial t} - F_5 \cdot \mathcal{L}_+ - F_7 \cdot \mathcal{L}_-}{F_2} \quad (32)$$

where:

$$F_1 = \frac{e_c}{\rho} \cdot \frac{P_t}{r T_t} \quad (33)$$

$$F_2 = \frac{T_t}{\rho} - \frac{e_c}{\rho C_p} \quad (34)$$

$$F_3 = \mathcal{L}_{t_1} u_{t_1} + \mathcal{L}_{t_2} u_{t_2} \quad (35)$$

$$F_4 = \left( -\frac{\rho c}{2} \cdot \frac{P_t}{P_s} + \frac{P_t}{r T_t} \cdot \left( \frac{\beta e_c}{2c} - \frac{u_n}{2} \right) \right) \quad (36)$$

$$F_5 = \left( -\frac{\beta T_t}{2c} + \frac{1}{C_p} \left( \frac{\beta e_c}{2c} - \frac{u_n}{2} \right) \right) \quad (37)$$

$$F_6 = \left( -\frac{\rho c}{2} \cdot \frac{P_t}{P_s} + \frac{P_t}{r T_t} \cdot \left( \frac{\beta e_c}{2c} + \frac{u_n}{2} \right) \right) \quad (38)$$

$$F_7 = \left( -\frac{\beta T_t}{2c} + \frac{1}{C_p} \left( \frac{\beta e_c}{2c} + \frac{u_n}{2} \right) \right) \quad (39)$$

Eq. (31) provides a relation between the right-going acoustic wave  $\mathcal{L}_+$  to impose and the incoming left-going  $\mathcal{L}_-$  wave from

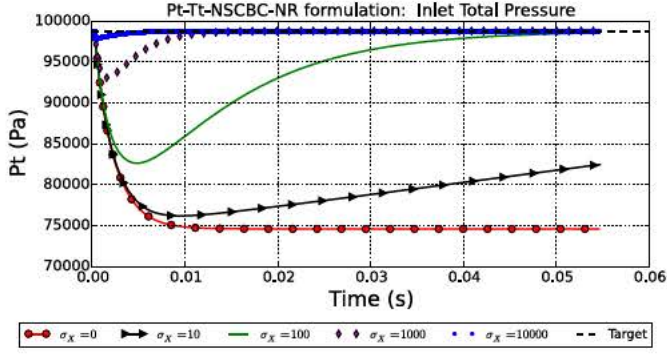


Fig. 5. Inlet total pressure  $P_t$  for various relaxation coefficients  $\sigma_x$ , for the Pt-Tt-NSCBC-NR formulation.

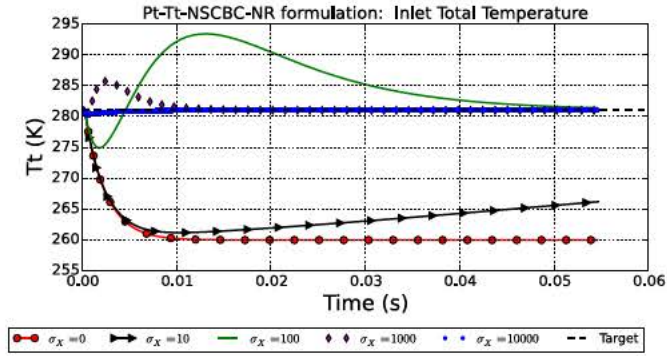


Fig. 6. Inlet total temperature  $T_t$  for various relaxation coefficients  $\sigma_x$ , for the Pt-Tt-NSCBC-NR formulation.

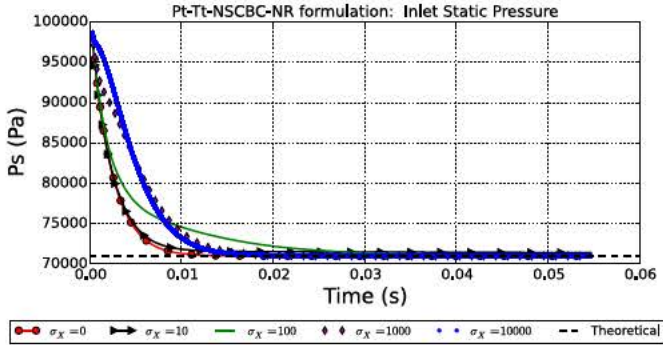


Fig. 7. Inlet static pressure  $P_s$  for various relaxation coefficients  $\sigma_x$ , for the Pt-Tt-NSCBC-NR formulation.

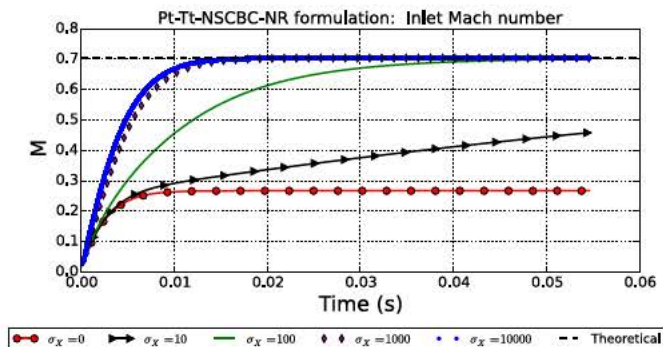


Fig. 8. Inlet Mach number  $M$  for various relaxation coefficients  $\sigma_x$ , for the Pt-Tt-NSCBC-NR formulation.

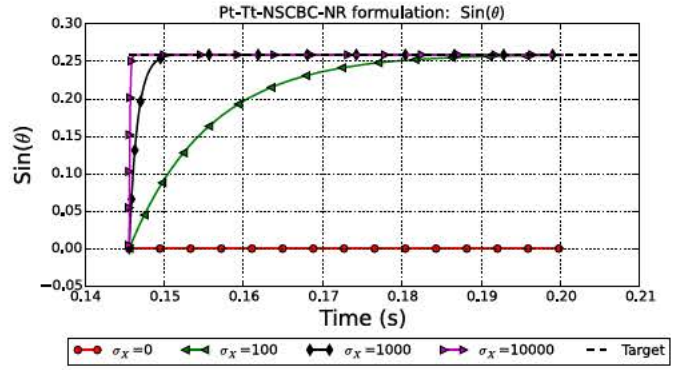


Fig. 9. Flow direction evolution.

the domain. This formulation is reflecting for acoustics, i.e.  $\mathcal{L}_+$  and  $\mathcal{L}_S$  are dependent on  $\mathcal{L}_-$ : Any non zero  $\mathcal{L}_-$  wave will induce a corresponding value for the incoming waves  $\mathcal{L}_+$  and  $\mathcal{L}_S$ . As pointed out by Guézennec and Poinso [19], a necessary non-reflecting condition requires that the ingoing wave  $\mathcal{L}_+$  does not depend on the outgoing one  $\mathcal{L}_-$ . This methodology is followed here, by setting  $\mathcal{L}_-$  to zero in Eq. (31) in order to ensure non-reflectivity.

$$\mathcal{L}_{t_1} = -\frac{\partial u_{t_1}}{\partial t} \quad (40)$$

$$\mathcal{L}_{t_2} = -\frac{\partial u_{t_2}}{\partial t} \quad (41)$$

$$\mathcal{L}_k = Y_k \mathcal{L}_S - \rho \frac{\partial Y_k}{\partial t} \quad (42)$$

$$\mathcal{L}_+ = \frac{F_1 \frac{\partial T}{\partial t} + F_2 \frac{\partial R}{\partial t} + \frac{R}{r} \cdot F_2 F_3 + \frac{1}{c_p} \cdot F_1 F_3 + F_1 \cdot \frac{T}{r} \sum_{k=1}^N r_k \frac{\partial Y_k}{\partial t}}{F_4 F_2 + F_5 F_1} \quad (43)$$

$$\mathcal{L}_S = \frac{\frac{\partial T}{\partial t} + \frac{1}{c_p} F_3 + \frac{T}{r} \sum_{k=1}^N r_k \frac{\partial Y_k}{\partial t} - F_5 \cdot \mathcal{L}_+}{F_2} \quad (44)$$

## 2.5. Practical implementation

Whenever implementing a non-reflective characteristic boundary condition, a well-known drawback is that they allow drifts of mean values which require a modification of the baseline theory. To avoid experiencing such a “drift” between the target value and the computed one, several authors have proposed linear relaxation methods. Rudy and Strikwerda [39] first proposed a methodology for a subsonic outlet, that is also adopted in Poinso and Lele [34], while Yoo et al. [53] proposed a similar approach for an inflow condition. More recently, Pirozzoli and Colonius [32] proposed a generalized relaxation method, involving the knowledge of the reference value at the first exterior (ghost) point. The linear relaxation approach is followed in this present work, writing any variable  $X$  temporal derivative as:

$$\frac{\partial X}{\partial t} dt = -\sigma_x (X_{predicted} - X_{target}) \quad (45)$$

where  $\sigma_x$  is a relaxation coefficient needed to be chosen by the user,  $X_{predicted}$  is the value of the variable  $X$  predicted by the numerical scheme, and  $X_{target}$  is the target value imposed by the boundary condition. These  $\frac{\partial X}{\partial t} dt$  are then used in Eqs. (40) to (44), with  $X$  being successively  $\sin(\theta)$ ,  $\sin(\phi)$ ,  $Y_k$ ,  $P_t$ ,  $T_t$ . The consequences of this relaxation method on the boundary acoustic behavior are detailed in Selle et al. [44] and Polifke et al. [35] who show that non zero values of  $\sigma_x$  lead to a boundary which is no longer

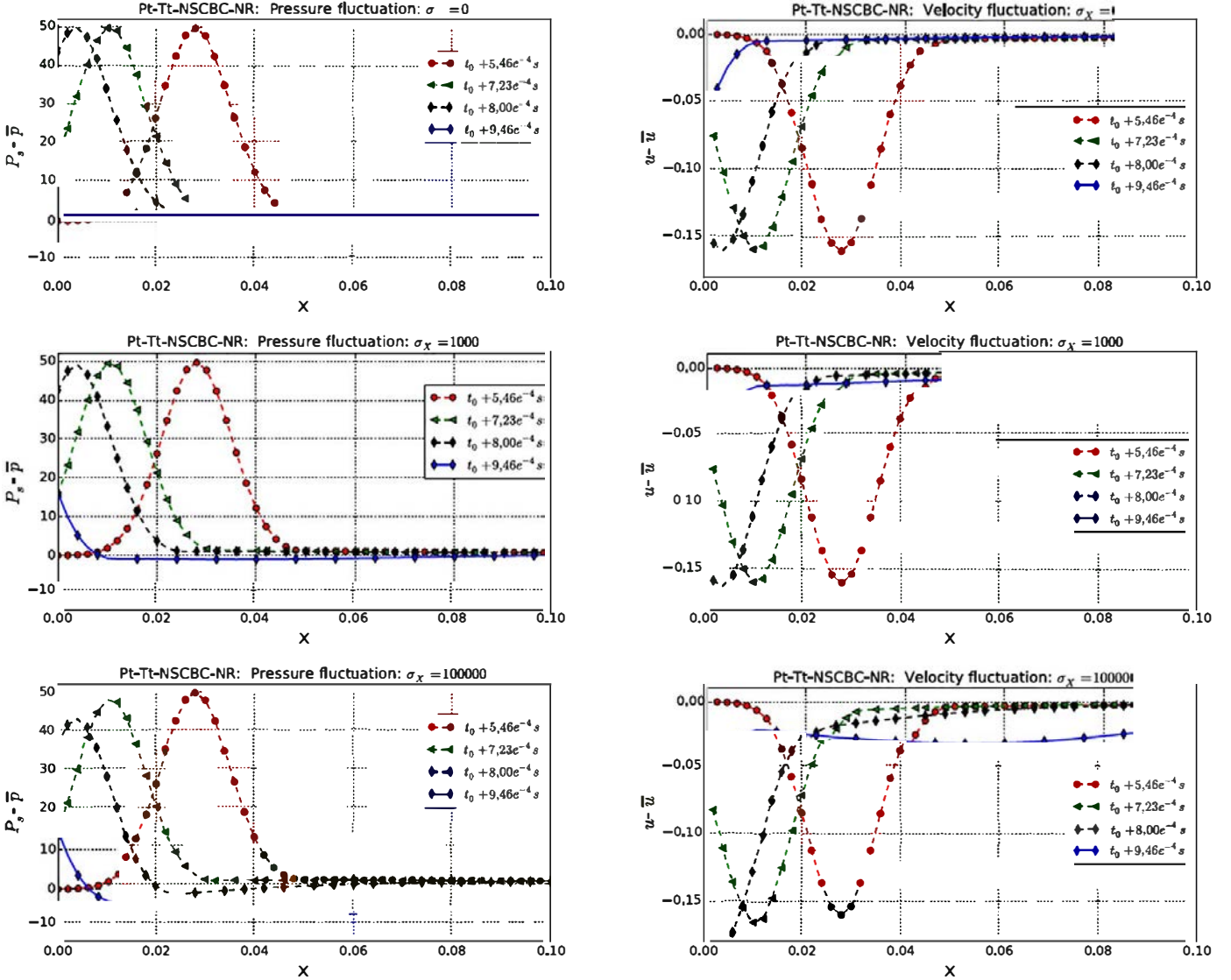


Fig. 10. Temporal evolution of the ingoing acoustic wave, for the Pt-Tt-NSCBC-NR formulation and for  $\sigma_X = 0$  (top),  $\sigma_X = 1000$  (middle),  $\sigma_X = 10,000$ ,  $\sigma_X = 100,000$  (bottom).  $\sigma_X = \sigma_{Pr} = \sigma_{Ti} = \sigma_{\sin(\theta)} = \sigma_{\sin(\phi)}$ . The acoustic wave maximum crosses the inlet boundary at  $t = t_0 + 8.41e^{-4}s$ .

“non-reflecting” but instead becomes “partially non-reflecting”, and therefore can be characterized by a reflecting coefficient  $R$  function of  $\sigma_X$ .

### 3. Validation and discussion


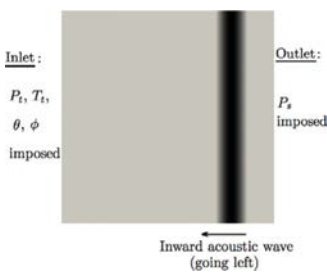
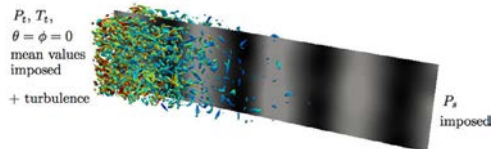

Two boundary conditions that impose  $P_t$ ,  $T_t$ , flow direction and species have been derived in Section 2.4, one being reflecting (Pt-Tt-NSCBC-R), the other being non-reflecting (Pt-Tt-NSCBC-NR). The aim of this paper is to evaluate the non-reflecting formulation, required for turbomachinery applications. Tests have also been performed to evaluate the reflecting formulation, but not shown here for the sake of concision. The current section allows evaluating the Pt-Tt-NSCBC-NR boundary conditions on several test-cases, and provides a best-practice to deal with relaxation coefficients which are the only adjustable parameters of the method. The first test-case (Section 3.1) consists in a 2D square-box with constant inlet  $P_t$ ,  $T_t$ , flow angles and constant static outlet pressure, and allows to investigate the flow establishment toward the imposed values for both conditions, depending on the relaxation coefficients. Once the flow is established for an axial case ( $\theta = \phi = 0$ ), Section 3.2 evaluates the effect of modifying the flow direction. The acoustic reflec-

tion coefficient of each conditions is then studied as a function of the relaxation coefficients  $\sigma_X$  in Section 3.3. The compatibility with a synthetic turbulence injection is finally evaluated in Section 3.4. To conclude, the derived boundary condition is used in a Nozzle Guide Vane flow simulation in Section 3.5. These test-cases are summarized in Table 2. Computations are performed using the 3D unstructured solver AVBP, detailed in Schönfeld et al. [42] and Gourdain et al. [17], using a two-step Taylor Galerkin TTGC (Colin and Rudgyard, [6]) numerical scheme.

#### 3.1. Convergence of the mean flow to imposed targets

The first academic test-case is a 2D test-case, with  $[L_x \times L_y] = [100 \text{ mm} \times 100 \text{ mm}]$ , discretized with  $[n_x \times n_y] = [128 \times 128]$  cells (Fig. 4). The inlet condition corresponds to a total pressure  $P_t = 98,803 \text{ Pa}$ , a total temperature  $T_t = 281 \text{ K}$ , a normal flow direction ( $\theta = \phi = 0$ ), for air. A static pressure  $P_s = 71,000 \text{ Pa}$  is imposed at the outlet boundary, and periodic conditions are applied on the other boundaries. For this case, the Mach number must reach a

**Table 2**  
Test-cases.

Test case	Schematic	Object of the study
2D square box		Flow setting up toward target values of $P_t$ , $T_t$ , $\theta$ , $\phi$ (subsections 3.1, 3.2).
2D square box		Acoustic wave impacting on inlet condition: reflectivity (subsection 3.3).
3D rectangular box		Turbulence injection: Turbulent characteristics, and non-reflectivity in case of turbulence injection (subsection 3.4).
Actual rotor-stator turbomachinery		Actual turbomachinery: Flow setting up toward target values, turbulence injection (subsection 3.5).

value given by ( $\gamma = 1.4$ ):

$$M = \sqrt{\frac{2}{\gamma - 1} \left( \left( \frac{P_t}{P_s} \right)^{\frac{\gamma - 1}{\gamma}} - 1 \right)} = 0.7036 \quad (46)$$

The initial solution is arbitrarily chosen, and characterized by a static pressure  $P_s = 98,803$  Pa, a static temperature  $T_s = 281$  K, and an initial velocity  $U = 10$  m/s. All relaxation coefficients are equal ( $\sigma_X = \sigma_{P_{tot}} = \sigma_{T_{tot}} = \sigma_{\sin(\theta)} = \sigma_{\sin(\phi)}$ ).

A probe is located at the inlet boundary condition, and the temporal evolutions of  $P_t$ ,  $T_t$  are given in Figs. 5 and 6 for the non-reflecting formulation. Figs. 7 and 8 display the inlet static pressure  $P_s$  and the inlet Mach number. As the configuration is periodic in the transverse direction, no loss occurs and the flow may be considered isentropic: the static pressure in the domain must be equal to the prescribed outlet static pressure. The inlet Mach number should reach the theoretical value of Eq. (46).

Figs. 5 to 8 show that  $\sigma_X = 0$  does not allow reaching the target value for this specific test-case for the non-reflecting formulation. When considering this phase of flow establishment, starting from an initial solution that differs from the final state, the user should use significant relaxation coefficient  $\sigma_X$  to rapidly converge the flow to the adequate and desired state. As evidenced by this test case, establishing a mean operating condition for a flow whose initial solution is a pure guess while imposing chosen boundary condition is not a simple problem. Clearly such a process is strongly dependant on the boundary condition formulation and the initial solution. Once the flow is established, tests show that the inlet relaxation coefficients  $\sigma_X$  can be brought back to zero and that no drift occurs. The corresponding established mean field is used in the following subsections as an initial condition:  $P_s = 71,000$  Pa,  $T_s = 255.711$  K,  $u = 225.99$  m/s,  $M = 0.7036$ .



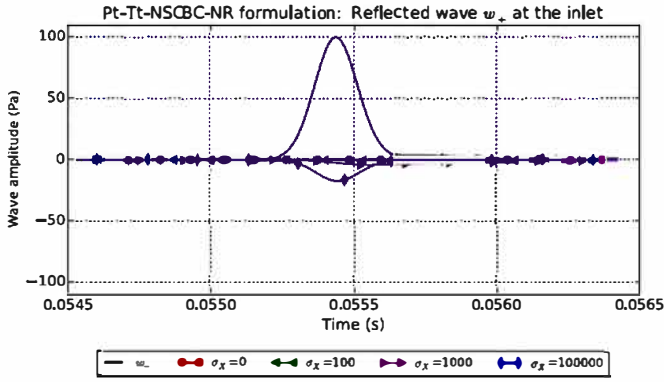


Fig. 11. Reflected wave  $w_+$ , depending on the relaxation coefficients  $\sigma_X$ , for non-reflecting formulation. The incoming left-going wave  $w_-$  is also depicted.

### 3.2. Imposition of a flow direction

Starting from the previously established flow, a velocity angle of  $\theta = 15^\circ$  is imposed at the boundary condition. Fig. 9, showing the time evolution of the flow direction, confirms that the proposed approach provides the correct evolution of  $\sin(\theta)$  toward the desired value ( $\sin(\theta) = 0.258$ ) when a non zero relaxation coefficient is used.

### 3.3. Acoustic properties of the inlet boundary conditions

The acoustic reflectivity of the proposed formulation is evaluated in this subsection, for various values of the relaxation coefficient  $\sigma_X$ . To do so, a Gaussian left-going acoustic wave is superimposed to the flow established in Section 3.1, initially centered at  $x_0 = \frac{x}{L} = \frac{3}{4}$ , and for which the following perturbation reads:

$$p' = -\rho c u' \quad \text{with} \quad u' = A e^{-\frac{(x-x_0)^2}{\Gamma^2}} \quad (47)$$

with  $A = 0.001$  and  $\Gamma = 0.01$ . Fig. 10 shows pressure and velocity fluctuation evolutions as the acoustic wave crosses the inlet boundary for several values of the  $\sigma_X$  coefficients for the non-reflecting formulation: very small reflections appear.

To quantitatively evaluate the reflection coefficient  $R$ , static pressure, velocity and density signals are recorded at the inlet probe and decomposed into mean and fluctuating components,

$$p(t) = \bar{p} + p'(t), \quad u(t) = \bar{u} + u'(t), \quad \rho(t) = \bar{\rho} + \rho'(t). \quad (48)$$

The inward and backward acoustic waves  $w_+$  and  $w_-$  are then reconstructed using:

$$\begin{cases} w_+ = p' + \rho c u' & (49a) \\ w_- = p' - \rho c u' & (49b) \end{cases}$$

Those waves are then recast into frequencies through a Fast Fourier Transform operator  $\hat{\cdot}$ , and the reflection coefficient  $R$  is finally obtained using:

$$R = \frac{\hat{w}_+}{\hat{w}_-} \quad (50)$$

Fig. 11 depicts the reconstructed reflected wave  $w_+$  at the inlet for several relaxation coefficients  $\sigma_X$ . Note that for a purely non-reflecting condition, although  $w_-$  is present,  $w_+$  should remain zero. Any signal in  $w_+$  reconstruction is therefore indicating of a reflection. For low values of  $\sigma_X$  (less than 100), the boundary behaves as expected: no reflection is observed for this non-reflecting formulation.

Fig. 13 depicts the evolution of the reflection coefficient for the considered working point, depending on the relaxation coefficient

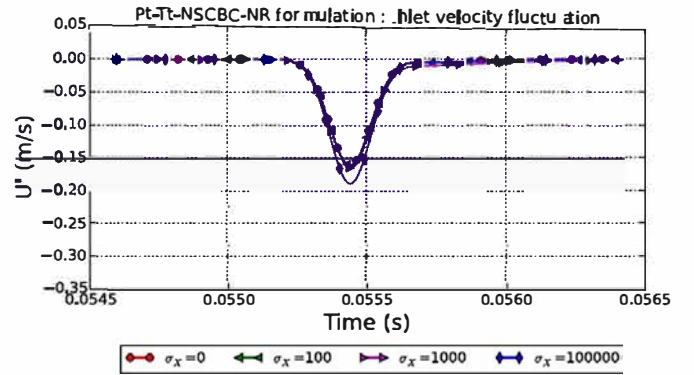
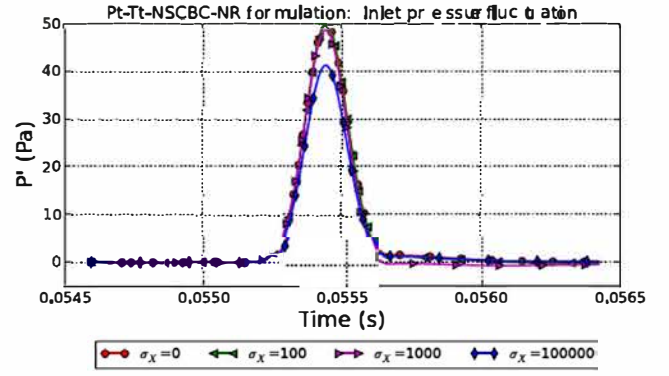


Fig. 12. Evolution of fluctuating pressure (top) and velocities (bottom) depending on the relaxation coefficients  $\sigma_X$ , for the non-reflecting formulation.

$\sigma_X$ . In this Figure, the maximum  $R$  is plotted for the Pt-Tt-NSCBC-NR formulation. For a zero relaxation coefficient, the proposed formulation behaves as expected. As  $\sigma_X$  increases, its behavior deteriorates.

The evolutions of  $P_t$  as the acoustic wave crosses the inlet are presented in Fig. 14. For  $\sigma_X = 0$ , the proposed non-reflecting formulation recovers the target  $P_t$  value as soon as the acoustic wave has passed the inlet. The same conclusion holds for the total temperature  $T_t$  (not shown).

### 3.4. Compatibility with turbulence injection

As stated in the introduction, an inlet boundary condition for turbomachinery computations must handle turbulence injection. Reviews of turbulence injection methodologies for LES may be found in Tabor and Baba-Ahmadi [46], Dhamankar et al. [11] and Wu [51]. The compatibility of the proposed non-reflecting boundary condition with a synthetic turbulence injection is assessed in this subsection as it is indeed a key condition for many turbomachinery computations.

The three unsteady velocity components ( $u'_1, u'_2, u'_3$ ) at the inlet are specified using a Kraichnan's approach [22]. Following the Vortical-Flow Characteristic Boundary Condition (VFCBC) proposed in Guézennec and Poinso [19], these fluctuations are added to the inlet acoustic waves derived in Section 2.4 and governing the mean flow, so that:

$$\mathcal{L}_{+turb} = \mathcal{L}_+ + \frac{\partial u'_1}{\partial x} \quad (51)$$

$$\mathcal{L}_{1turb} = \mathcal{L}_{t1} + \frac{\partial u'_2}{\partial x} \quad (52)$$

$$\mathcal{L}_{2turb} = \mathcal{L}_{t2} + \frac{\partial u'_3}{\partial x} \quad (53)$$

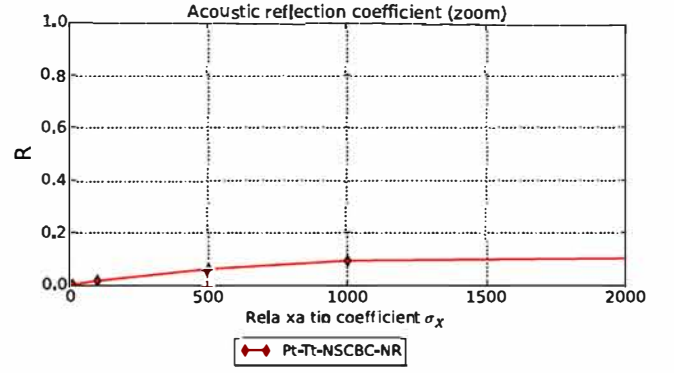
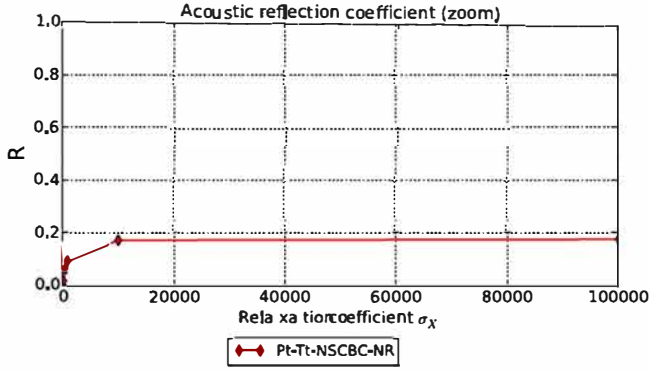


Fig. 13. Evolution of the reflection coefficient  $R$  depending on the relaxation coefficient  $\sigma_x$  for the reflecting and the non-reflecting formulation.

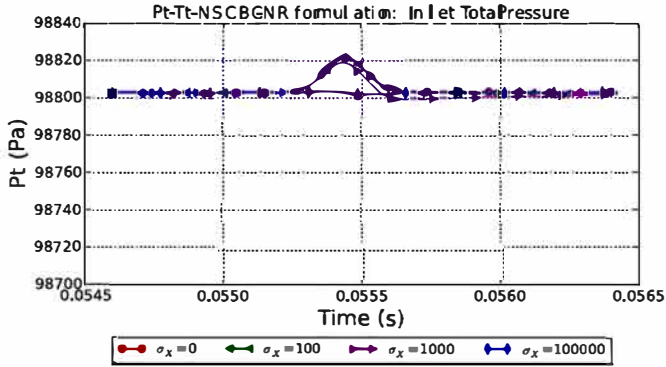


Fig. 14. Evolution of total pressure  $P_t$  as the left-going wave  $w_-$  crosses the inlet, for the non-reflecting formulation.

For the validation of the proposed methodology, a turbulent convected flow in a rectangular box is computed, for which the inflow mean inlet  $P_t$ ,  $T_t$ , as well as an additional synthetic inlet turbulence are imposed (Fig. 15). The computational domain is a  $[L_x \times L_y \times L_z] = [4 \text{ mm} \times 1 \text{ mm} \times 1 \text{ mm}]$  rectangular box, discretized with  $[n_x \times n_y \times n_z] = [392 \times 98 \times 98]$  cells. Total pressure and temperature  $P_t$  and  $T_t$  are imposed at the inlet, static pressure  $P_s$  is imposed at the outlet, so that the expected mean velocity is  $u = 95 \text{ m/s}$ . All other boundaries are periodic conditions. The inlet velocity fluctuation is  $u' = 5.0 \text{ m/s}^{-1}$ , ( $TKE = \frac{3}{2}u'^2 = 37.5 \text{ m}^2\text{s}^{-2}$ ). The target integral lengthscale is  $\lambda = \frac{\sqrt{2\pi}}{k_e} = \frac{\lambda_e}{\sqrt{2\pi}} = 0.56 \text{ mm}$ , with  $k_e$  the most energetic wavenumber in the Passot-Pouquet spectrum, and  $\lambda_e$  the most energetic lengthscale. 1000 modes are used to build the inlet velocity fluctuation field. Fig. 15 shows the injection of vortical structures near the inlet (on the left), whose sizes

are spatially increasing when convected to the exit (on the right), as expected from a spatially decaying turbulent flow.

First, the integral turbulent timescale  $t_{turb}$  and lengthscale  $\lambda$  are evaluated as a function of the channel axial length using the two-time correlation  $R_{uu}(x, \tau)$  (Pope [36]):

$$t_{turb}(x) = \int_{\tau=0}^{\tau=\tau_{max}} R_{uu}(x, \tau) d\tau. \quad (54)$$

Where  $\tau_{max}$  is such that  $R_{uu}(x, \tau_{max}) = 0$ . From this turbulent timescale, an integral turbulent lengthscale is deduced using Taylor's hypothesis (Taylor, [47]). This hypothesis consists in considering a "frozen turbulence" advected by the mean flow, and enables the integral lengthscale evaluation through the knowledge of the integral timescale. It is valid for an established mean flow, and if  $\frac{u'}{u} \ll 1$ . This hypothesis is very often used in experimental works and has been shown to fairly predict turbulence scales (Dahm and Southerland [9]). Some authors however raised limitations for some flows configurations, as Lin [25] who showed this hypothesis is no longer valid for high shear flows, or Lee et al. [23] who showed that this hypothesis does not apply for the dilatational part of turbulence. More recent works also show this hypothesis breaks down for wall-bounded flows (Del Alamo and Jiménez [10], Moin [28]). Finally:

$$\lambda = u \cdot t_{turb} \quad (55)$$

Fig. 16 displays the turbulent kinetic energy decrease expected within the domain (a), and the turbulent integral lengthscale (b). At the inlet, a value of  $TKE = 35 \text{ m}^2\text{s}^{-2}$  is reached, very close to the imposed value  $TKE = 37.5 \text{ m}^2\text{s}^{-2}$ . A similar conclusion can be drawn for the integral turbulent lengthscale at the inlet. It can be noticed that  $\lambda$  starts decreasing, then increases as expected. The primary decrease in  $\lambda$  is associated to the adaptation length required to reach a physical turbulent spectrum.

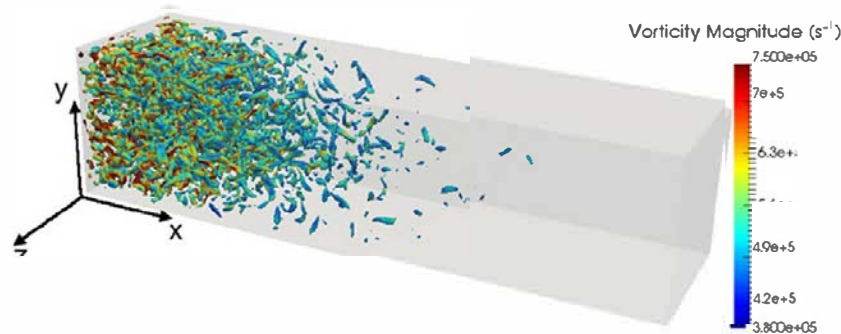
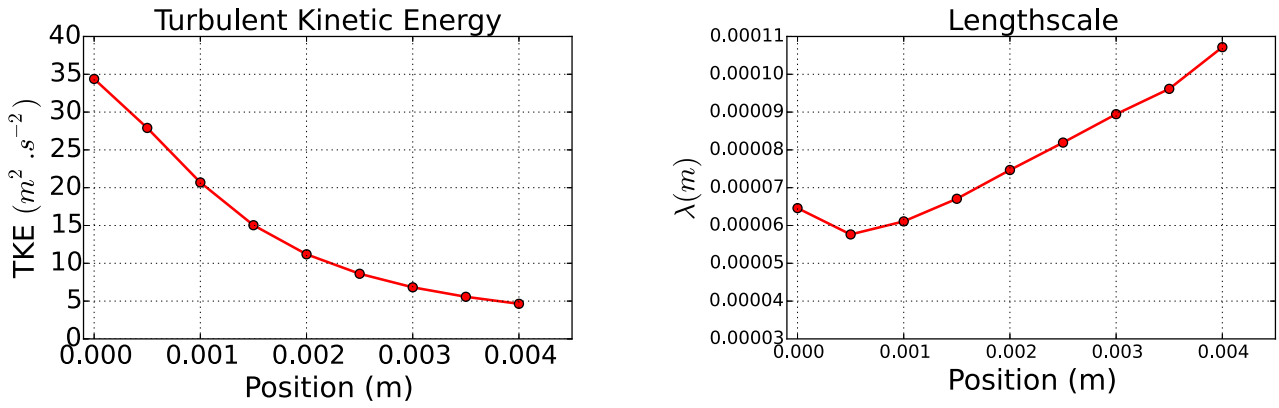


Fig. 15. Synthetic turbulence injection: contours of  $Q$  criterion colored by vorticity magnitude. The flow is going from the left to the right. Inlet: Pt-Tt-NSCBC-NR.



(a) Turbulent kinetic Energy along the channel. (b) Evaluated integral turbulent lengthscale along the channel.

Fig. 16. Turbulent kinetic energy (left) and integral lengthscale  $\lambda$  (right) along the x-axis (Fig 15).

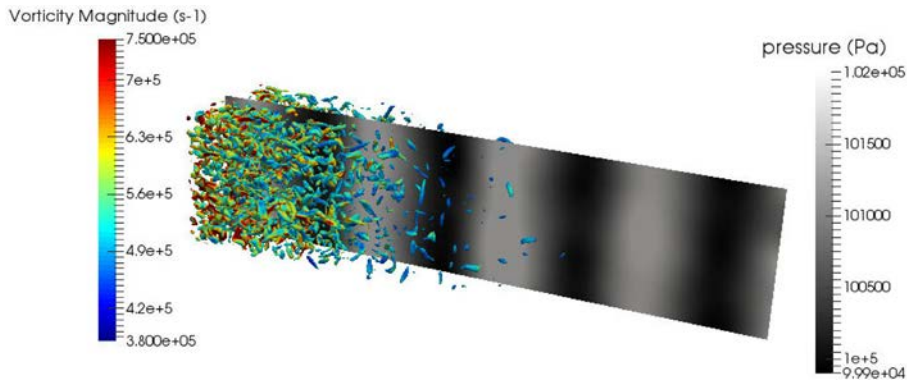


Fig. 17. Interaction between synthetic turbulence and acoustic waves: instantaneous contours of Q criterion colored by vorticity magnitude, and cut colored by the pressure field. The flow is going from the left to the right, acoustic waves travel from right to left. Inlet: Pt-Tt-NSCBC-NR.

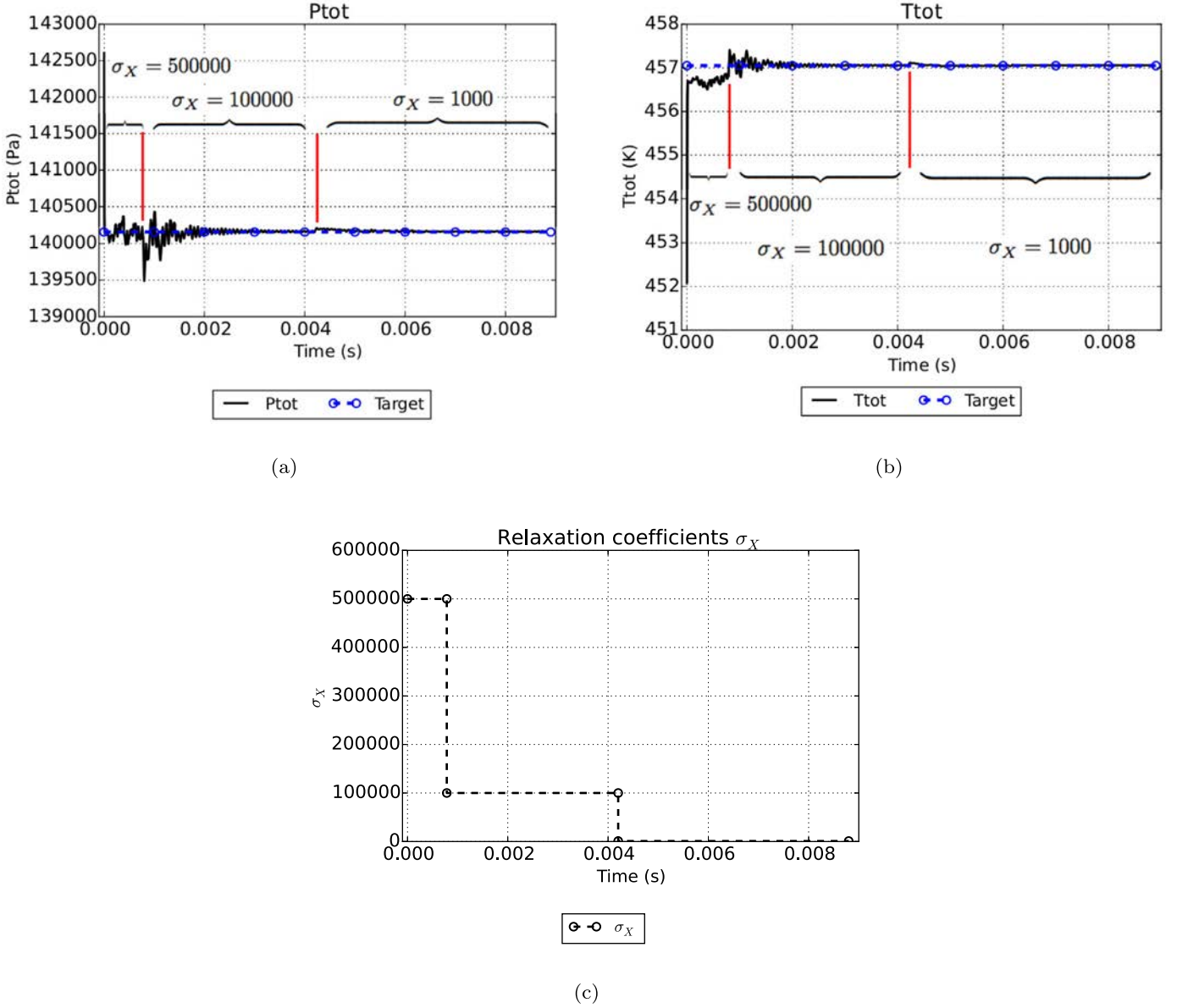


Fig. 18. FACTOR turbine stage configuration.

As stated in Eqs. (51) to (53), fluctuations are added to waves imposing the mean flow, on which the relaxation methodology is applied. In practice, velocity fluctuations modify the local mach number, and thus local values of  $P_t$  and  $T_t$ . Increasing  $\sigma_X$  will consequently induce a damping in the resulting average kinetic energy. This might be a reason for the small difference found above

( $TKE = 35 \text{ m}^2 \cdot \text{s}^{-2}$  instead of  $TKE = 37.5 \text{ m}^2 \cdot \text{s}^{-2}$ ). Note that the effect of  $\sigma_X$  on the resulting turbulence will increase as the turbulent velocity fluctuations will result in large Mach number fluctuations.

To evaluate the acoustic behavior in the case of turbulence injection, a harmonic pulsation is imposed at the outlet of an estab-



**Fig. 19.** Temporal evolution of integrated variables over the inlet boundary condition toward the target values, together with the relaxation coefficients used during the simulation. The last value used for  $\sigma_X$  is  $\sigma_X = 1000$ .

lished mean flow, leading to a pressure perturbation that varies in time, reading:

$$p_{ac}(t) = p_{ac0} \sin(2\pi \cdot f_{ac} \cdot t) \quad (56)$$

The chosen frequency is  $f_{ac} = 260$  kHz, and the pressure amplitude is  $p_{ac0} = 1000$  Pa, and  $\sigma_X = 0$ . An instantaneous contour of Q-criterion, the second invariant of the velocity gradient tensor, and a longitudinal plane colored by the pressure field are shown in Fig. 17. Harmonic acoustic waves travel from the outlet to the inlet, and the evaluated acoustic reflection coefficient  $R$  at the inlet Eq. (50) is  $R = 0.06$ , proving the ability of the Pt-Tt-NSCBC-NR to inject turbulence while remaining quasi non-reflecting. The turbulent characteristics are found to be the same as those shown in Fig. 16.

Since the Pt-Tt-NSCBC-NR formulation is satisfying on these academic test-cases, it is then tested in an industrial configuration in the following subsection.

### 3.5. Turbomachinery configuration

The turbine stage belonging to the non-reactive axial combustor simulator FACTOR (Full Aerothermal Combustor-Turbine interactions Research) configuration (Fig. 18), is computed using the Pt-Tt non-reflecting boundary condition (Pt-Tt-NSCBC-NR), and the LES solver TurboAVBP described in Wang et al. [49] enabling the rotor relative motion in a LES context. The configuration consists in 2 stator vanes and 3 rotor blades, with a rotating speed of 8500 rpm, on a 76 millions cells mesh. The initial solution consists in a uniform field, with a static pressure of  $P_s = 149,000$  Pa, a static temperature  $T_s = 450$  K, and no initial velocity. A 2D-map of  $P_t$ ,  $T_t$  and flow direction is imposed at the inlet. More details about the FACTOR configuration may be found in Duchaine et al. [12].

The temporal evolutions of the averaged values of  $P_t$  and  $T_t$  over the inlet patch are shown in Fig. 19, as well as the relaxation coefficients  $\sigma_X$  used during the simulation. High  $\sigma_X$  are needed during the flow setting up, and these coefficients are decreased once the target values are reached.

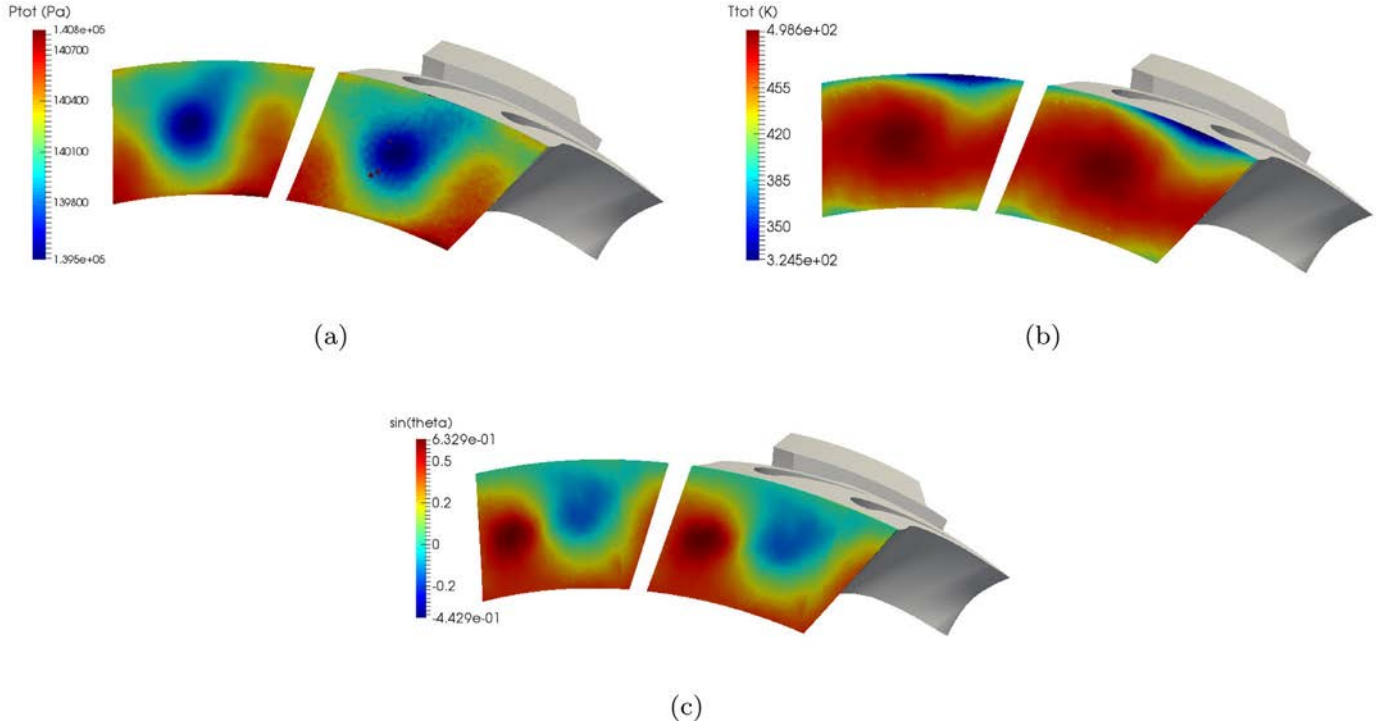


Fig. 20. Inlet total pressure (a), total temperature (b) and flow direction (c) for an actual turbine stage. Imposed solution on left, time averaged solution over 1.9ms on right.

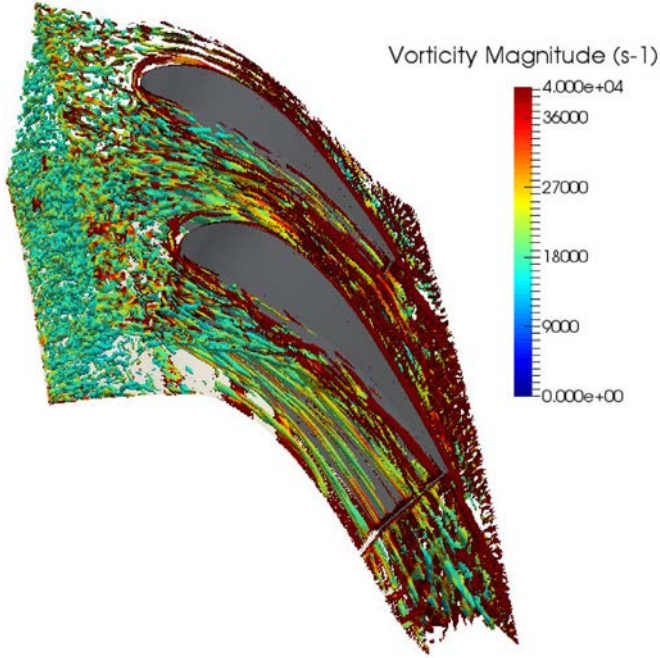


Fig. 21. Isosurface of Q-criterion colored by vorticity.

Fields of  $P_t$ ,  $T_t$ , and flow direction  $\sin(\theta)$  imposed by the boundary condition and fields obtained by the LES are compared in Fig. 20, showing the ability of the Pt-Tt-NSCBC-NR to correctly handle such spatial 2D-maps prescriptions. Finally, a turbulence injection is added. To do so, a velocity fluctuation of  $u' = 5$  m/s is imposed, with an integral lengthscale  $\lambda = \frac{\sqrt{2\pi}}{k_e} = \frac{\lambda_e}{\sqrt{2\pi}} = 1.23$  mm. The resulting mean fluctuation measured at the inlet is  $u' = 4.33$  m/s, and the integral lengthscale is  $\lambda = 1.17$  mm. The resulting

flow is depicted in Fig. 21, showing turbulent structures interacting with the inlet guide vane.

#### 4. Conclusions

An extension of the Navier–Stokes Characteristic Boundary Condition (NSCBC) is proposed in this paper to impose total pressure  $P_t$ , total temperature  $T_t$ , flow angles  $\theta$  and  $\phi$ , and multi-species composition  $Y_k$  at the inlet of a compressible LES or DNS.

Following the NSCBC methodology, the compressible expressions of total pressure and total temperature are derived to be expressed in terms of characteristic waves  $\mathcal{L}_i$ . Those  $\mathcal{L}_i$  amplitudes are then obtained using Locally One-Dimensional Inviscid (LODI) relations for situations where  $P_t$ ,  $T_t$ ,  $\theta$ ,  $\phi$  and  $Y_k$  are imposed. Two formulations are proposed: the first is reflecting (Pt-Tt-NSCBC-R), the other one non-reflecting (Pt-Tt-NSCBC-NR). Both formulations are implemented using a linear relaxation methodology.

These two formulations are evaluated on several test-cases, for a large range of relaxation coefficients. Results show that a large range of relaxation coefficients enable to recover a quasi reflecting or a quasi non-reflecting behavior as well as non-drifting mean values. The compatibility of the Pt-Tt-NSCBC-NR condition with turbulence injection is then demonstrated for a turbomachinery simulation. A synthetic turbulence injection is added to the proposed formulation, and validated on a turbulent periodic rectangular box. The inlet boundary condition leads to fair results regarding the expected turbulent kinetic energy, and turbulent integral lengthscale at the inlet. The non-reflectivity in case of turbulence injection is also demonstrated.

Finally, this boundary condition is tested for a turbomachinery configuration. The FACTOR turbine stage is chosen and spatial 2D map of total quantities and flow direction is imposed, together with a synthetic turbulence field. This test-case shows the ability of the proposed Pt-Tt-NSCBC-NR to reach the inlet  $P_t$ ,  $T_t$ , and flow angle target values, and to handle the 2D-map prescription and the turbulent characteristics at the inlet of a complex geometry.

## Acknowledgments

The authors wish to acknowledge the support of the STAE foundation via the RTRA project SIMACO3FI for financial support. The computational resources for the actual turbomachinery simulation were provided by the GENCI network, and were part of the allocation no. A0022A06074 (CINES-OCIGEN). The first author also acknowledges Luis-Miguel Segui for fruitful discussions about turbulence injection, and Jérôme de Laborderie for code verification.

## Appendix

### 5.1. Useful relations

Eqs. (57) to (64) are useful relations resulting from LODI relations and their combinations. Those relations may be found in [37].

$$r = \sum_{k=1}^N r_k Y_k \quad (57)$$

$$\frac{\partial u_n}{\partial t} + \frac{1}{2}(\mathcal{L}_+ + \mathcal{L}_-) = 0 \quad (58)$$

$$\frac{\partial u_{t_1}}{\partial t} + \mathcal{L}_{t_1} = 0 \quad (59)$$

$$\frac{\partial u_{t_2}}{\partial t} + \mathcal{L}_{t_2} = 0 \quad (60)$$

$$\frac{\partial P_s}{\partial t} = -\frac{\rho c}{2}(\mathcal{L}_+ + \mathcal{L}_-) \quad (61)$$

$$\frac{\partial r}{\partial t} = -\frac{1}{\rho} \left( -r \mathcal{L}_s + \sum_{k=1}^N r_k \mathcal{L}_k \right) \quad (62)$$

$$\frac{\partial T_s}{\partial t} = -\frac{\beta T_s}{2c}(\mathcal{L}_+ + \mathcal{L}_-) + \frac{T_s}{\rho r} \sum_{k=1}^N r_k \mathcal{L}_k \quad (63)$$

$$\frac{\partial Y_k}{\partial t} = -\frac{1}{\rho}(\mathcal{L}_k - Y_k \mathcal{L}_s) \quad (64)$$

### 5.2. Kinetic energy derivation

The temporal derivation of  $P_t$  and  $T_t$  involves the Mach number  $M$  derivation, which itself involves the kinetic energy  $e_c$  equation derivation:

$$e_c = \frac{u_n^2 + u_{t_1}^2 + u_{t_2}^2}{2} \quad (65)$$

The kinetic energy temporal derivative is:

$$\frac{\partial e_c}{\partial t} = u_n \frac{\partial u_n}{\partial t} + u_{t_1} \frac{\partial u_{t_1}}{\partial t} + u_{t_2} \frac{\partial u_{t_2}}{\partial t} \quad (66)$$

Using Eqs. 58–60, the kinetic energy temporal derivative is finally:

$$\frac{\partial e_c}{\partial t} = -\frac{u_n}{2}(\mathcal{L}_+ - \mathcal{L}_-) - u_{t_1} \mathcal{L}_{t_1} - u_{t_2} \mathcal{L}_{t_2} \quad (67)$$

### 5.3. Square Mach number derivation

The square Mach number yields:

$$M^2 = \frac{u_n^2 + u_{t_1}^2 + u_{t_2}^2}{\gamma r T_s} = \frac{2e_c}{\gamma r T_s} \quad (68)$$

Using Eqs. (67), (62), (63), the square Mach number temporal derivative finally writes:

$$\begin{aligned} \frac{\partial M^2}{\partial t} = & \frac{2}{c^2} \left( \mathcal{L}_+ \cdot \left( \frac{\beta e_c}{2c} - \frac{u_n}{2} \right) + \mathcal{L}_- \cdot \left( \frac{\beta e_c}{2c} + \frac{u_n}{2} \right) - u_{t_1} \mathcal{L}_{t_1} \right. \\ & \left. - u_{t_2} \mathcal{L}_{t_2} - \frac{e_c}{\rho} \cdot \mathcal{L}_s \right) \end{aligned} \quad (69)$$

### 5.4. Total pressure derivation

The total pressure  $P_t$  is defined by:

$$P_t = P_s \left( 1 + \frac{\beta}{2} M^2 \right)^{\left( \frac{\gamma}{\beta} \right)} \quad (70)$$

Its temporal derivatives gives:

$$\frac{\partial P_t}{\partial t} = \frac{\partial P_s}{\partial t} \left( 1 + \frac{\beta}{2} M^2 \right)^{\left( \frac{\gamma}{\beta} \right)} + P_s \frac{\gamma}{\beta} \frac{\beta}{2} \cdot \frac{\partial M^2}{\partial t} \left( 1 + \frac{\beta}{2} M^2 \right)^{\left( \frac{\gamma}{\beta} - 1 \right)} \quad (71)$$

The total temperature  $T_t$  expression is:

$$\frac{T_t}{T_s} = \left( 1 + \frac{\beta}{2} M^2 \right) \quad (72)$$

Using Eq. (61) and Eq. (69), the total pressure derivative, written in terms of  $\mathcal{L}_i$ , is finally:

$$\begin{aligned} \frac{\partial P_t}{\partial t} = & \mathcal{L}_+ \cdot \left( -\frac{\rho c}{2} \frac{P_t}{P_s} + \frac{P_t}{r T_t} \left( \frac{\beta e_c}{2c} - \frac{u_n}{2} \right) \right) + \mathcal{L}_- \cdot \left( -\frac{\rho c}{2} \frac{P_t}{P_s} \right. \\ & \left. + \frac{P_t}{r T_t} \cdot \left( \frac{\beta e_c}{2c} + \frac{u_n}{2} \right) \right) \\ & - \mathcal{L}_{t_1} u_{t_1} \cdot \frac{P_t}{r T_t} - \mathcal{L}_{t_2} u_{t_2} \cdot \frac{P_t}{r T_t} - \frac{e_c}{\rho} \cdot \mathcal{L}_s \cdot \frac{P_t}{r T_t} \end{aligned} \quad (73)$$

### 5.5. Total temperature derivation

The total temperature temporal derivative is:

$$\frac{\partial T_t}{\partial t} = \frac{\partial T_s}{\partial t} \cdot \frac{T_t}{T_s} + T_s \cdot \frac{\beta}{2} \cdot \frac{\partial M^2}{\partial t} \quad (74)$$

This equation is developed using Eqs. (63) and (69) :

$$\begin{aligned} \frac{\partial T_t}{\partial t} = & \mathcal{L}_+ \cdot \left( -\frac{\beta T_t}{2c} + \frac{1}{C_p} \left( \frac{\beta e_c}{2c} - \frac{u_n}{2} \right) \right) \\ & + \mathcal{L}_- \cdot \left( -\frac{\beta T_t}{2c} + \frac{1}{C_p} \left( \frac{\beta e_c}{2c} + \frac{u_n}{2} \right) \right) - \mathcal{L}_{t_1} \frac{u_{t_1}}{C_p} - \mathcal{L}_{t_2} \frac{u_{t_2}}{C_p} \\ & + \frac{T_t}{\rho r} \sum_{k=1}^N r_k \mathcal{L}_k - \frac{e_c}{\rho C_p} \cdot \mathcal{L}_s \end{aligned} \quad (75)$$

### 5.6. System resolution

$\mathcal{L}_+$ ,  $\mathcal{L}_s$  and  $\mathcal{L}_k$  are determined solving the system of unknowns given by Eqs. (73), (75) and (64). The term  $\sum_{k=1}^N r_k \mathcal{L}_k$  in Eq. (75) needs to be expressed. Eq. (64) gives:

$$\mathcal{L}_k = Y_k \mathcal{L}_s - \rho \frac{\partial Y_k}{\partial t} \quad (76)$$

Multiplying Eq. (76) by  $\sum_{k=1}^N r_k$ , and using Eqs. (57) and (10) yields:

$$\sum_{k=1}^N r_k \mathcal{L}_k = r \mathcal{L}_S - \rho \sum_{k=1}^N r_k \frac{\partial Y_k}{\partial t} \quad (77)$$

The expression of  $\sum_{k=1}^N r_k \mathcal{L}_k$  given in Eq. (77) can be injected in Eq. (75). The system of unknowns becomes Eqs. (78)–(80):

$$\begin{aligned} \mathcal{L}_+ \cdot \left( -\frac{\rho c}{2} \cdot \frac{P_t}{P_s} + \frac{P_t}{r T_t} \cdot \left( \frac{\beta e_c}{2c} - \frac{u_n}{2} \right) \right) - \frac{e_c}{\rho} \cdot \mathcal{L}_S \cdot \frac{P_t}{r T_t} \\ = \frac{\partial P_t}{\partial t} + \frac{P_t}{r T_t} \cdot (\mathcal{L}_{t_1} u_{t_1} + \mathcal{L}_{t_2} u_{t_2}) - \mathcal{L}_- \cdot \left( -\frac{\rho c}{2} \frac{P_t}{P_s} \right. \\ \left. + \frac{P_t}{r T_t} \cdot \left( \frac{\beta e_c}{2c} + \frac{u_n}{2} \right) \right) \end{aligned} \quad (78)$$

$$\begin{aligned} \mathcal{L}_+ \cdot \left( -\frac{\beta T_t}{2c} + \frac{1}{C_p} \left( \frac{\beta e_c}{2c} - \frac{u_n}{2} \right) \right) + \mathcal{L}_S \cdot \left( \frac{T_t}{\rho} - \frac{e_c}{\rho C_p} \right) \\ = \frac{\partial T_t}{\partial t} + \frac{1}{C_p} \cdot (\mathcal{L}_{t_1} u_{t_1} + \mathcal{L}_{t_2} u_{t_2}) + \frac{T_t}{r} \sum_{k=1}^N r_k \frac{\partial Y_k}{\partial t} \\ - \mathcal{L}_- \cdot \left( -\frac{\beta T_t}{2c} + \frac{1}{C_p} \left( \frac{\beta e_c}{2c} + \frac{u_n}{2} \right) \right) \end{aligned} \quad (79)$$

$$\frac{\partial Y_k}{\partial t} = -\frac{1}{\rho} (\mathcal{L}_k - Y_k \mathcal{L}_S) \quad (80)$$

Using the expressions defined in Eqs. (33) to (39), the system of unknowns can be rewritten:

$$\begin{cases} \mathcal{L}_+ \cdot F_4 - \mathcal{L}_S \cdot F_1 & = \frac{\partial P_t}{\partial t} + \frac{P_t}{r T_t} F_3 - \mathcal{L}_- \cdot F_6 & (a) \\ \mathcal{L}_+ \cdot F_5 + \mathcal{L}_S \cdot F_2 & = \frac{\partial T_t}{\partial t} + \frac{1}{C_p} F_3 + \frac{T_t}{r} \sum_{k=1}^N r_k \frac{\partial Y_k}{\partial t} - \mathcal{L}_- \cdot F_7 & (b) \\ \frac{\partial Y_k}{\partial t} & = -\frac{1}{\rho} (\mathcal{L}_k - Y_k \mathcal{L}_S) & (c) \end{cases} \quad (81)$$

Combining equations Eqs. (81a) and (81b) provides a single equation, with a single unknown  $\mathcal{L}_+$ , removing the unknown  $\mathcal{L}_S$ . Eq. (81a)  $\times F_2 +$  Eq. (81b)  $\times F_1$  gives :

$$\begin{aligned} \mathcal{L}_+ \cdot (F_4 F_2 + F_5 F_1) & = F_2 \frac{\partial P_t}{\partial t} + F_1 \frac{\partial T_t}{\partial t} + \frac{P_t}{r T_t} \cdot F_3 F_2 + \frac{1}{C_p} \cdot F_3 F_1 \\ & + F_1 \cdot \frac{T_t}{r} \sum_{k=1}^N r_k \frac{\partial Y_k}{\partial t} - \mathcal{L}_- (F_6 F_2 + F_1 F_7) \end{aligned} \quad (82)$$

$\mathcal{L}_+$  is finally deduced:

$$\mathcal{L}_+ = \frac{F_1 \frac{\partial T_t}{\partial t} + F_2 \frac{\partial P_t}{\partial t} + \frac{P_t}{r T_t} \cdot F_3 F_2 + \frac{1}{C_p} \cdot F_3 F_1 + F_1 \cdot \frac{T_t}{r} \sum_{k=1}^N r_k \frac{\partial Y_k}{\partial t} - \mathcal{L}_- (F_6 F_2 + F_1 F_7)}{F_4 F_2 + F_5 F_1} \quad (83)$$

Once  $\mathcal{L}_+$  has been expressed, the unknown  $\mathcal{L}_S$  wave is deduced from Eq. (81b):

$$\mathcal{L}_S = \frac{\frac{\partial T_t}{\partial t} + \frac{1}{C_p} F_3 + \frac{T_t}{r} \sum_{k=1}^N r_k \frac{\partial Y_k}{\partial t} - F_5 \cdot \mathcal{L}_+ - F_7 \cdot \mathcal{L}_-}{F_2} \quad (84)$$

## References

- [1] Albin E, D'Angelo Y, Vervisch L. Flow streamline based Navier–Stokes characteristic boundary conditions: modeling for transverse and corner outflows. *Comput Fluids* 2011;51(1):115–26.
- [2] Anker J., Schrader B., Seybold U., Mayer J., Casey M. A three-dimensional non-reflecting boundary condition treatment for steady-state flow simulations. In: *Proceedings of the forty-fourth AIAA aerospace sciences meeting and exhibit*. January 2006; Reno, Nevada. ISBN 978-1-62410-039-0; 2006.
- [3] Baum M, Poinso T, Thévenin D. Accurate boundary conditions for multicomponent reactive flows. *J Comput Phys* 1994;116:247–61.

- [4] Carullo JS, Nasir S, Cress RD, Ng WF, Thole KA, Zhang LJ, et al. The effects of freestream turbulence, turbulence length scale, and exit Reynolds number on turbine blade heat transfer in a transonic cascade. *J Turbomach* 2011;133(1):011030.
- [5] Choi J, Teng S, Han J-C, Ladeinde F. Effect of free-stream turbulence on turbine blade heat transfer and pressure coefficients in low Reynolds number flows. *Int J Heat Mass Transf* 2004;47(14–16):3441–52.
- [6] Colin O, Ruggyard M. Development of high-Order TaylorGalerkin schemes for LES. *J Comput Phys* 2000;162(2):338–71.
- [7] Colonius T. Numerically nonreflecting boundary and interface conditions for compressible flow and aeroacoustic computations. *AIAA J* 1997;35(7):1126–33.
- [8] Colonius T. Modelling artificial boundary conditions for compressible flow. *Annu Rev Fluid Mech* 2004;36(1):315–45.
- [9] Dahm WJ, Southerland KB. Experimental assessment of Taylor's hypothesis and its applicability to dissipation estimates in turbulent flows. *Phys Fluids* 1997;9(October 1996):2101–7.
- [10] Del Álamo JC, Jiménez J. Estimation of turbulent convection velocities and corrections to Taylor's approximation. *J Fluid Mech* 2009;640:5–26.
- [11] Dhamankar N.S., Blaisdell G.A., Lyrantzis A.S. An overview of turbulent inflow boundary conditions for large eddy simulations (Invited). In: *Proceedings of the twenty-second aiaa computational fluid dynamics conference*. JUNE. ISBN 978-1-62410-366-7; 2015, p. 1–28.
- [12] Duchaine F, Dombard J, Gicquel LY, Koupper C. On the importance of inlet boundary conditions for aerothermal predictions of turbine stages with large eddy simulation. *Comput Fluids* 2017;154:60–73.
- [13] Freund JB. Proposed inflow/outflow boundary condition for direct computation of aerodynamic sound. *AIAA J* 1997;35(4):740–2.
- [14] Germano M. Turbulence: the filtering approach. *J Fluid Mech* 1992;238:325–36.
- [15] Giles M. Non-reflecting boundary conditions for euler equation calculations. *AIAA J* 1990;28(12):2050–8.
- [16] Giles MB. UNSFLO: A numerical method for unsteady inviscid flow in turbomachinery. Tech. Rep.. Gas Turbine Laboratory, MIT; 1988.
- [17] Gourdain N, Gicquel L, Montagnac M, Vermorel O, Gazaix M, Staffelbach G, et al. High performance parallel computing of flows in complex geometries: I. Methods. *Comput Sci Discov* 2009;2(1):015003.
- [18] Granet V, Vermorel O, Léonard T, Gicquel L, Poinso T. Comparison of non-reflecting outlet boundary conditions for compressible solvers on unstructured grids. *AIAA J* 2010;48(10):2348–64.
- [19] Guézennec N, Poinso T. Acoustically nonreflecting and reflecting boundary conditions for vorticity injection in compressible solvers. *AIAA J* 2009;47(7):1709–22.
- [20] Jahanmiri M. Boundary layer transitional flow in gas turbines. Tech. Rep.. Göteborg, Sweden: Dpt. Appl. Mech., Chalmers University of Technology; 2011.
- [21] Koupper C, Poinso T, Gicquel LYM, Duchaine F. Compatibility of characteristic boundary conditions with radial equilibrium in turbomachinery simulations. *AIAA J* 2014;52(12):2829–39.
- [22] Kraichnan RH. Diffusion by a random velocity field. *Phys Fluids* 1970;13(1):22.
- [23] Lee S, Lele SK, Moin P. Simulation of spatially evolving turbulence and the applicability of Taylor's hypothesis in compressible flow. *Phys Fluids A* 1992;4(7):1521–30.
- [24] Leonard A. Energy cascade in large-eddy simulations of turbulent fluid flows. *Adv Geophys* 1974;18(PA):237–48.
- [25] Lin C. On Taylor's hypothesis and the acceleration terms in the Navier–Stokes equations. *Q Appl Math* 1953;10(4):295–396.
- [26] Lodato G, Domingo P, Vervisch L. Three-dimensional boundary conditions for direct and large-eddy simulation of compressible viscous flows. *J Comput Phys* 2008;227(10):5105–43.
- [27] Michelassi V, Chen L-W, Pichler R, Sandberg RD. Compressible direct numerical simulation of low-Pressure turbinespart II: Effect of inflow disturbances. *J Turbomach* 2015;137(7):071005.
- [28] Moin P. Revisiting Taylor's hypothesis. *J Fluid Mech* 2009;640:1–4.
- [29] Moureau V, Lartigue G, Sommerer Y, Angelberger C, Colin O, Poinso T. Numerical methods for unsteady compressible multi-component reacting flows on fixed and moving grids. *J Comput Phys* 2005;202(2):710–36.
- [30] Nicoud F. Defining wave amplitude in characteristic boundary conditions. *J Comput Phys* 1999;149(2):418–22.
- [31] Okong'o N, Bellan J. Consistent boundary conditions for multicomponent real gas mixtures based on characteristic waves. *J Comput Phys* 2002;176(2):330–44.
- [32] Pirozzoli S, Colonius T. Generalized characteristic relaxation boundary conditions for unsteady compressible flow simulations. *J Comput Phys* 2013;248:109–26.
- [33] Poinso T, Veynante D. *Theoretical and numerical combustion*. 3rd; 2012.
- [34] Poinso TJ, Lele SK. Boundary conditions for direct simulations of compressible viscous flows. *J Comput Phys* 1992;101(1):104–29.
- [35] Polifke W, Wall C, Moin P. Partially reflecting and non-reflecting boundary conditions for simulation of compressible viscous flow. *J Comput Phys* 2006;213(1):437–49.
- [36] Pope S. *Turbulent flows*. Cambridge University Press; 2000.
- [37] Porta M. Développement, vérification et validation des outils les pour l'étude du bruit de combustion et de l'interaction combustion / acoustique / turbulence. Institut National Polytechnique de Toulouse; 2007. Ph.D. thesis.
- [38] Prosser R. Improved boundary conditions for the direct numerical simulation of turbulent subsonic flows. I. Inviscid flows. *J Comput Phys* 2005;207(2):736–68.

- [39] Rudy H, Strikwerda JC. A nonreflecting outflow boundary condition for subsonic Navier–Stokes calculations. *J Comput Phys* 1980;36:55–70.
- [40] Saxer A.P., Giles M.B., Saxer A. P., Giles M.B.. Quasi-three-dimensional non-reflecting boundary conditions for Euler equations calculations. In: Proceedings of the tenth computational fluid dynamics conference. 1603-CP; Honolulu, USA; 1991, p. 845–857.
- [41] Schlüß D., Frey C., Ashcroft G.. Consistent non-reflecting boundary conditions for both steady and unsteady flow simulations in turbomachinery applications. In: Proceedings of the VII European congress on computational methods in applied sciences and engineering. June; Crete Island, Greece; 2016, p. 5–10.
- [42] Schönfeld T, Rudgyard M. Steady and unsteady flows simulations using the hybrid flow solver avbp. *AIAA J* 1999;37:1378–85.
- [43] Scillitoe AD, Tucker PG, Adami P. Numerical investigation of three-Dimensional separation in an axial flow compressor: the influence of freestream turbulence intensity and endwall boundary layer state. *J Turbomach* 2016;139(2). 0210111–10
- [44] Selle L, Nicoud F, Poinot T. Actual impedance of nonreflecting boundary conditions: implications for computation of resonators. *AIAA J* 2004;42(5):958–64.
- [45] Struijs R, Rudgyard M, Nicoud F, Hernandez G. A set of characteristic boundary conditions for the cell-vertex AVBP code. Tech. Rep.. CERFACS, TR/CFD/96/09; 1996.
- [46] Tabor GR, Baba-Ahmadi MH. Inlet conditions for large eddy simulation: a review. *Comput Fluids* 2010;39(4):553–67.
- [47] Taylor G. The spectrum of turbulence. Proceedings of the royal society of London A: mathematical. *Phys Eng Sci* 1938;164(919):476–90.
- [48] Thompson KW. Time dependent boundary conditions for hyperbolic systems. *J Comput Phys* 1987;68(1):1–24.
- [49] Wang G, Duchaine F, Papadogiannis D, Duran I, Moreau S, Gicquel L. An over-set grid method for large eddy simulation of turbomachinery stages. *J Comput Phys* 2014;274:333–55.
- [50] Wissink JG, Zaki TA, Rodi W, Durbin PA. The effect of wake turbulence intensity on transition in a compressor cascade. *Flow Turbul. Combust.* 2014;93(4):555–76.
- [51] Wu X. Inflow turbulence generation methods. *Annu Rev Fluid Mech* 2017;49(1):23–49.
- [52] Yoo CS, Im HG. Characteristic boundary conditions for simulations of compressible reacting flows with multi-dimensional, viscous and reaction effects. *Combust Theor Model* 2007;11(2):259–86.
- [53] Yoo CS, Wang Y, Trouvé A, Im HG. Characteristic boundary conditions for direct simulations of turbulent counterflow flames. *Combust Theor Model* 2005;9(4):617–46.